THE SEISMOLOGICAL SOCIETY OF AMERICA
400 Evelyn Ave., Suite 201
Albany, CA 94706-1375
(510) 525-5474; FAX (510) 525-7204
www.seismosoc.org

Bulletin of the Seismological Society of America, Vol. 106, No. 1, pp. 158–173, February 2016, doi: 10.1785/0120150184

Developing an Application-Specific Ground-Motion Model for Induced Seismicity

by Julian J. Bommer, Bernard Dost, Benjamin Edwards, Peter J. Stafford, Jan van Elk, Dirk Doornhof, and Michail Ntinalexis

Abstract A key element of quantifying both the hazard and risk due to induced earthquakes is a suite of appropriate ground-motion prediction equations (GMPEs) that encompass the possible shaking levels due to such events. Induced earthquakes are likely to be of smaller magnitude and shallower focal depth than the tectonic earthquakes for which most GMPEs are derived. Furthermore, whereas GMPEs for moderate-to-large magnitude earthquakes are usually derived to be transportable to different locations and applications, taking advantage of the limited regional dependence observed for such events, the characteristics of induced earthquakes warrant the development of application-specific models. A preliminary ground-motion model for induced seismicity in the Groningen gas field in The Netherlands is presented as an illustration of a possible approach to the development of these equations. The GMPE is calibrated to local recordings of small-magnitude events and captures the epistemic uncertainty in the extrapolation to larger magnitude considered in the assessment of the resulting hazard and risk.

Introduction

Induced and triggered seismicity resulting from anthropogenic activities are currently receiving heightened attention due to the increased incidence of such earthquakes, which are accompanied by greater public concern and regulatory scrutiny. This places an onus on the operators of the inducing activities to quantify and limit the potential impact of earthquakes, either through the use of "traffic light" systems that aim to control the resulting hazard (Bommer *et al.*, 2006; Häring *et al.*, 2008; Bachmann *et al.*, 2011; Majer *et al.*, 2012; Zoback, 2012; Mena *et al.*, 2013; Douglas and Aochi, 2014; Mignan *et al.*, 2015) or through a more holistic risk mitigation strategy (Bommer *et al.*, 2015). In either case, the essential elements in quantifying the potential impact of such earthquakes on exposed population and building stock are ground-motion prediction equations (GMPEs) or ground-motion models. Because induced earthquakes are generally of smaller magnitude and shallower focal depth than the ranges typically covered by GMPEs derived for tectonic seismicity, the resulting ground motions are more likely to exhibit differences from one location or region to another than may be the case for natural earthquakes by virtue of sensitivity to the heterogeneous nature of the upper crust. On the basis of this premise, we believe it is desirable to develop application-specific GMPEs rather than generic equations for ground motions due to induced earthquakes.

In this article, we present preliminary GMPEs for the Groningen gas field in The Netherlands, where hydrocarbon production is causing earthquake activity that has prompted the need for quantification—and mitigation—of the consequent risk to the affected population. The equations represent the current status in an ongoing scope of development for these models, but we believe the experience and insights obtained, as well as some of the innovations implemented, may be useful to others faced with the need to construct ground-motion models as part of the quantification due to induced earthquakes elsewhere. The article begins with a brief overview of some of the issues associated with deriving GMPEs for induced earthquakes and discusses some of the models that have been proposed to date. The remainder of this article then explains the derivation of the models for the median predictions of spectral acceleration (SA) and the associated aleatory variability for the specific case of induced seismicity in Groningen. We conclude with a brief discussion of the ongoing work to further refine the Groningen GMPEs and offer some conclusions regarding the experience obtained in deriving the equations presented herein.

GMPEs for Induced Earthquakes

Before presenting the derivation of new GMPEs for the Groningen field, we briefly discuss some of the challenges associated with developing equations for estimating ground motions from induced earthquakes, and we consider different options for addressing these challenges.

Challenges and Opportunities

Historically, the main impetus for the development of GMPEs has been the need to estimate earthquake ground motions for consideration in seismically resistant design; this has resulted in a focus on larger earthquakes (moment magnitude, $\mathbf{M} > \sim 5$). Modeling the hazard and risk due to induced earthquakes requires a focus on lower-magnitude ranges, and this represents the first and most immediate challenge, not least because it has been well established that empirical GMPEs generally do not extrapolate reliably to smaller magnitudes (Bommer *et al.*, 2007; Atkinson and Morrison, 2009). The second challenge is directly associated with the first, namely that regional differences in ground-motion characteristics become more apparent at smaller magnitudes (e.g., Chiou *et al.*, 2010). The third challenge is the issue of focal depth, because induced earthquakes tend to be associated with hypocenters in the upper 5 km of the crust, whereas tectonic earthquakes tend to be distributed over greater depth ranges. The shallow foci of induced earthquakes also results in the wave propagation paths being more strongly influenced by the heterogeneous properties of the uppermost portion of the crust, which can be expected to further accentuate regional differences. This is particularly the case for the Groningen gas field given the presence of a high-velocity salt layer above the reservoir, as discussed later. At the same time, there is another factor that may often facilitate the option of developing application-specific ground-motion models: given the nature of the projects causing induced seismicity, it is not uncommon to have a relatively detailed level of understanding of this upper-crustal structure.

Although the challenges are formidable, it is also worth noting that there may be some other features of induced seismicity that offer opportunities that are not so easily accessible when deriving GMPEs for natural (tectonic) earthquakes. The most important of these is that the equations, if derived for a specific application, will tend to focus on an area in close proximity to the activity causing the earthquakes. Consequently, there will be many cases in which the earthquakes are effectively occurring within a single seismic source and propagating along a narrow range of travel paths, allowing nonergodic standard deviations (sigma) to be used (e.g., Atkinson, 2006; Lin *et al.*, 2011; Rodriguez-Marek *et al.*, 2013).

Another interesting opportunity arises with induced seismicity due to the much higher frequency of occurrence of induced events with respect to natural seismicity. Provided the area of the project is adequately instrumented, there can therefore be an opportunity to frequently update and improve GMPEs—and reduce associated epistemic uncertainties—for the specific application.

Existing GMPEs for Induced Seismicity

To date, relatively few GMPEs have been proposed for induced seismicity, although it is reasonable to expect more models to be put forward as focus on this topic continues to increase. Dost *et al.* (2004) published GMPEs for peak ground acceleration (PGA) and peak ground velocity (PGV) derived from recordings of shallow induced earthquakes in The Netherlands. This would therefore seem to be a very logical choice for application to the Groningen gas field, but residual analyses showed that this equation is a very poor predictor of the Groningen ground motions (Bourne *et al.*, 2015). This anomalous behavior has been interpreted as the result of the thick, high-velocity Zechstein salt layer that overlies the Groningen gas reservoir but which is located below the reservoir in the Roswinkel gas field, from which the majority of recordings used by Dost *et al.* (2004) were obtained. This fact gives further weight to our argument that application-specific GMPEs must be developed for induced seismicity.

Sharma *et al.* (2013), following earlier work by Convertito *et al.* (2012) for PGA, recognized the need for application-specific GMPEs and derived predictive equations for PGA, PGV, and SA for induced earthquakes in The Geysers geothermal field in California. The equation is a function of magnitude and hypocentral distance (R_{hyp}), with a station-specific correction for site response. The data used to derive the equation are from earthquakes with magnitudes in the **M** 1.3–3.3 range, and there is no indication that the equation could be applied to larger events. This is an important issue—and potentially another challenge in addition to those addressed in the previous section—because hazard and risk assessments will almost inevitably require extrapolation to magnitudes larger than those that have been observed. This challenge is addressed in the study by Douglas *et al.* (2013), which uses a large database of recordings mostly, but not exclusively, from recordings of induced earthquakes to derive empirical and stochastic equations. The latter are used to extrapolate the predictions to larger magnitudes, subsequently fitted to functional forms for convenience, whereas the empirical models inform the sigma values. The stochastic simulation-based models cover many combinations of values of the Brune (1970, 1971) stress parameter, Q, and kappa (Anderson and Hough, 1984), in order to provide a framework for capturing epistemic uncertainty. However, in common with the Convertito *et al.* (2012) model, they obtain rather large standard deviations ($\sigma[\ln(\text{PGA})] = 1.30$), possibly as a result of limited site classification information. As explained later, the approach we adopted for the Groningen field has many similarities with that used by Douglas *et al.* (2013) but uses only application-specific data.

The recent study by Atkinson (2015) addresses the magnitude extrapolation in another way by directly performing regressions on recordings from tectonic, rather than induced, earthquakes in the **M** 3–6 range, obtained at hypocentral distances of less than 40 km. In common with the other studies discussed above, the sigma values were once again found to be rather large ($\sigma[\ln(\text{PGA})] = 0.85$). The applicability of the equations to any specific case of induced earthquakes would clearly need to be determined using local data; however, in instances where no such data existed, these equations (like

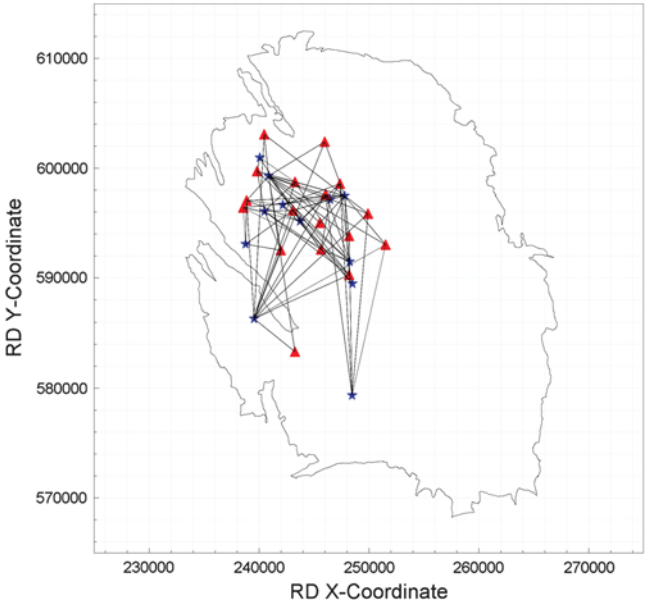

Figure 1. Locations of Royal Netherlands Meteorological Institute (KNMI) accelerograph stations (red triangles) and epicenters (blue stars) of the earthquakes in the database; coordinates (in meters) are defined by the Dutch Rijks-Driehoek (RD) system. Thin line shows the boundary of the Groningen gas field; for location, see Bourne *et al.* (2015).

those from Douglas *et al.*, 2013) could be included to capture epistemic uncertainty.

GMPEs for the Groningen Field

GMPEs are generally derived so that they can be applied in broad regions or even globally for earthquakes in a particular type of tectonic environment. For induced seismicity, however, we believe that the magnitude range of interest and the sensitivity to the structure of the upper few kilometers of the crust, combined with the lower stress drops expected for shallow earthquakes, obliges the development of application-specific GMPEs. The fact that Dutch GMPEs derived from recordings of induced earthquakes in another gas field were found to be unable to predict the motion recorded in the Groningen field, despite the common magnitude range, provides clear support for this position.

For the preliminary probabilistic seismic-hazard analysis (PSHA) conducted in support of the 2013 Winningsplan (gas production license application for the Groningen field), a single predictive equation was developed for PGA and PGV. The approach taken to develop these equations, which were necessarily conservative because there was no scope for a logic-tree formulation in that initial study, was to adopt a GMPE derived from tectonic earthquakes, and make adjustments to the coefficients when applied below a certain magnitude threshold such that the extrapolations to smaller events matched the recorded motions from the field (Bourne *et al.*, 2015). The sigma value from the original tectonic

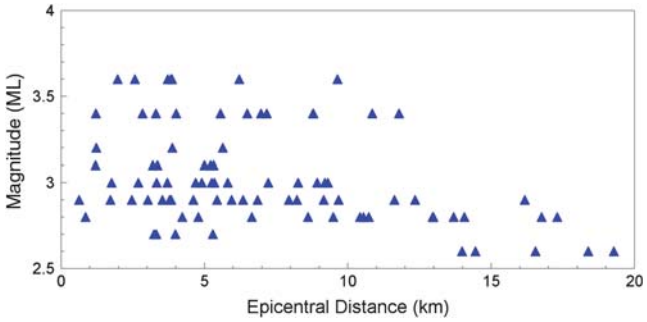

Figure 2. Magnitude–distance distribution of the Groningen database used in this study.

GMPE was assumed to apply across the full magnitude range, which extends from **M** 2.5 to 6.5, the lower value being the smallest events found to contribute to the hazard estimates and the larger value the upper limit considered in the risk integrations. This rather crude initial model has now been replaced with a model that is better calibrated to local conditions and also captures the epistemic uncertainty in the predictions, as explained in the following sections.

Model for Median Ground-Motion Predictions

Whereas the initial GMPEs for PGA and PGV for Groningen were obtained by extrapolating an existing GMPE to match the local recordings in the small-magnitude range, the new equations are developed directly from the field data and extended to larger magnitudes using stochastic simulations.

Ground-Motion Database

The database used to derive the equations is composed of 85 accelerograms recorded by the Royal Netherlands Meteorological Institute (KNMI) strong-motion network, which consists of 18 instruments located at surface stations within the Groningen field (Fig. 1). The accelerograms were obtained from 12 earthquakes with magnitudes ranging from **M** 2.6 to 3.6 at epicentral distances of up to 20 km (Fig. 2).

The magnitudes are assigned based on the assumption that the local magnitudes (M_L) assigned by KNMI are equivalent to **M** in this range. We justify this assumption based on the fact that the magnitudes used in this study are greater than the magnitude where the expected 1:1 scaling (Deichmann, 2006) between local and moment magnitudes breaks down due to the effects of attenuation (Grünthal *et al.*, 2009; Goertz-Allmann *et al.*, 2011). The validity of this assumption is a subject of ongoing research, but it is not necessarily a critical issue given that the hazard and risk calculations are based on a seismological model invoking the same assumption (Bourne *et al.*, 2014). All stations are located on soft soil deposits with V_{S30} (time-averaged shear-wave velocity in the top 30 m) values estimated to be about 180–210 m/s. Only the horizontal components of motion

were considered in this study, using the geometric mean of the two components.

The preliminary risk calculations to be undertaken by Nederlandse Aardolie Maatschappij B.V. (NAM), for which these equations were generated, only required SAs at periods of 0.01 s (assumed equivalent to PGA) and 0.2, 0.5, 1, and 2 s, because the current fragility functions were developed in terms of these five ground-motion parameters only.

Explanatory Variables and Functional Form

The initial phase of the GMPE development was to fit a simple functional form to the data using random effects maximum-likelihood regressions (Pinheiro and Bates, 2004). The only explanatory variables included in the model are magnitude and epicentral distance R_{epi}, which was adopted in place of R_{hyp} because the earthquakes are all assumed to occur within the gas reservoir (of thickness on the order of 150–300 m), located at a depth of 3 km. Because the earlier equation (Bourne *et al.*, 2015) was adapted from a GMPE derived for tectonic earthquakes, the use of R_{hyp} was essential because the focal depth distribution of those events did not match the shallow foci of the Groningen earthquakes, but there is no need to explicitly model the constant focal depth for the new equations derived directly from local data. Moreover, the use of R_{epi} greatly simplifies the sigma correction for the use of a point-source approximation at larger magnitudes, as described later. Earthquakes in the Groningen field are the result of either normal or strike-slip faulting; however, in the absence of reliable fault-plane solutions for the 12 earthquakes in the database, it was not possible to model the influence of the style of faulting. No explicit term for site response was included because the work to determine the dynamic characteristics of the near-surface deposits in the field is not yet sufficiently advanced; see the Discussion and Conclusions section. The entire area of interest for the hazard and risk study is overlain by soft soils with V_{S30} values in a relatively narrow range; indications are that locations in the north of the field, where most of the accelerographs are located, are softer than those in the south, making the use of network-averaged site amplification function conservative when linear site response is being considered.

The GMPE's functional form was chosen as follows, including a magnitude-dependent near-source distance saturation term (e.g., Yenier and Atkinson, 2014) that also serves to capture the magnitude dependence of geometric spreading (e.g., Cotton *et al.*, 2008):

$$\ln(Y) = c_1 + c_2\mathbf{M} + c_4 \ln\sqrt{R_{epi}^2 + [\exp(c_5\mathbf{M} + c_6)]^2}, \quad (1)$$

in which Y is the geometric mean SA at 5% of critical damping. The coefficient c_3 was reserved for nonlinear magnitude scaling to be added later; the purpose of this simple empirical model was geared toward exploration of the functional form and constraint of the variability components. Because the data cover a rather limited distance range, no attempt was made to also include a term to explicitly represent the effects of anelastic attenuation. Performing the regressions for the five coefficients at each period individually led to unphysical combinations of c_5 and c_6 at longer periods. In order to resolve this problem, a more complex regression was performed across the five periods simultaneously with the constraint of common values for these two coefficients, which were obtained as 0.4233 and −0.6083, respectively. In passing, we note that these coefficients yield a near-source saturation distance term that is almost identical to an alternative value to the Yenier and Atkinson (2014) considered by Atkinson (2015). Period-dependent estimates of the other coefficients and variance components were also obtained in this first stage. However, for the final model, the other three coefficients (c_1, c_2, and c_4) were subsequently obtained from period-by-period regressions with these two values held constant. The standard deviations were found to be between 0.51 and 0.58 in natural logarithmic units.

Although equation (1) was found to provide a good fit to the data, it is clear from the functional form that the model would not extrapolate reliably to larger magnitudes because the scaling is purely linear: at the upper limit of magnitudes considered for the Groningen seismic hazard and risk assessments, the linear magnitude scaling yields unfeasibly high accelerations. In order to be able to extend the predictions up to **M** 6.5, it was decided to make use of stochastic simulations (Hanks and McGuire, 1981; Boore, 1983, 2003). To this end, it was first necessary to obtain estimates of source, path, and site parameters from inversion of the Fourier amplitude spectra of the recordings.

Source, Path, and Site Parameters from Inversions

The procedure of Edwards *et al.* (2008) was applied to the Fourier amplitude spectra of the 85 recordings of Groningen ground motions to estimate the parameters of the theoretical point-source spectrum required for the stochastic simulations. In view of the relatively small database and the strong trade-offs that can exist between these parameters, as many of these as possible were constrained independently of the inversions. Kappa values were estimated using the high-frequency fitting approach of Anderson and Hough (1984), applied to the interval from 10 Hz to the highest frequency at which the signal-to-noise ratio was above 4, which led to a network average estimate of 0.05 s, consistent with the average value of 0.06 s from the broadband spectral fit. A network average site amplification function was obtained as part of the broadband spectral inversions, which is consistent with the decision not to include site-specific amplification in the current GMPEs. Geometric spreading was assumed to be $1/R_{hyp}$, based on the fact that the value of coefficient c_4 in equation (1) was very close to 1 at longer periods (where

the effect of Q would not be expected to be strong). The inversions yielded average estimates of 260 and 150 for Q (frequency independent with reference velocity 3.5 km/s) from broadband and high-frequency fitting, respectively. Estimates of the event-specific stress parameter ranged from 0.1 to 50 bars, with an event average of 7 bars (and record average of 9 bars).

From these initial findings, 36 different simulation models were proposed based on combinations of geometrical spreading ($1/R_{hyp}^{1.0}$ or $1/R_{hyp}^{1.1}$), Q at reference velocity 3.5 km/s (150 and 250), site kappa (κ_0) (0.05, 0.06, and 0.07 s), and stress parameter (10, 30, or 90 bars; with 2.6 km/s being the shear-wave velocity within the reservoir) along with the network-average site amplification function. Simulations were performed, using the program SMSIM (Boore, 2005), with duration based on the source (reciprocal of the corner frequency) and path (0.05 R_{hyp}; Herrmann, 1985) contributions. The simulated response spectral ordinates were compared with the recorded motions and the misfit and variance were averaged across the five oscillator periods to yield a single measure of bias and spread for each combination of simulation parameters. The best fitting model of the 36 was found to have geometric spreading of $1/R_{hyp}$, $Q = 150$, $\kappa_0 = 0.06$ s, and a stress parameter of 30 bars. Simulations with these parameters yielded predicted SAs in good agreement with the median values obtained from the empirical GMPE equation (1) (Fig. 3).

A point worthy of discussion here is why the best estimate of the stress parameter for the central model is 30 bars, whereas the average value obtained from the inversions was just 7 bars. Partly, as explained above, this arises from the fact that in the simulations, a search is conducted for combination of parameters providing the best fit to the data rather than considering each parameter in isolation. However, we believe that the main reason for this apparent discrepancy is that the inversions are performed in terms of hypocentral distance, whereas in the simulations the empirical magnitude-dependent near-source distance saturation term is imposed. This leads to reduction of the predicted motions at short distances, which requires an increase in the stress parameter to match the recorded amplitudes.

Stochastic Simulations for Larger Magnitudes and Epistemic Uncertainty

Using these source, path, and site parameters, simulations could easily be run to obtain estimates of the response spectral ordinates over the entire magnitude range of interest up to **M** 6.5. However, it must be recognized that the farther the models are pushed from the magnitude range covered by the data (**M** 2.6–3.6), the greater the epistemic uncertainty. Therefore, instead of a single suite of simulations, we opted for three separate sets in order to better capture the epistemic uncertainty associated with the predictions at larger magnitudes. The stress parameter is varied in these simulations, adopting two alternative values in addition to the central estimate of 30 bars. The lower model was assigned a stress parameter of 10 bars; and, for the upper model, the stress parameter increased from 30 bars to a constant value of 100 bars for **M** 4.5 and greater. The latter model is chosen to be consistent with ground motions from tectonic earthquakes; similar magnitude-dependent stress parameter models have been used by others (e.g., Rietbrock *et al.*, 2013). The relationship between the estimated stress parameter values and these three models is illustrated in Figure 4.

Examples of the resulting predictions are shown in Figure 5, from which it can be appreciated that the formulation results in a very modest spread at lower magnitudes (reflecting the fact that although the model is reasonably well constrained for **M** 2.6–3.6, the fit currently relies on a relatively small database) that increases with magnitude to reflect the inevitable epistemic uncertainty that results from the absence of local data. The three models are assigned to logic-tree branches, with the largest weight assigned to the central model based on a stress parameter of 30 bars.

Some discussion is warranted for the justification of this rather low central value. From analysis of intensity data obtained for tectonic and induced earthquakes in the central and eastern United States, Hough (2014) inferred that stress drops from the latter are systematically lower. Hough (2014) attributed this observation to the shallower depths of induced events, with the consequence that in the epicentral region the reduction of motions due to lower stress drop may be balanced out by the shorter travel paths. The concept of lower stress drops for shallower crustal earthquakes has also been proposed for tectonic earthquakes: for example, Allen *et al.* (2006) found very low stress drops for very shallow earthquakes in western Australia, and the shallow-focus 2012 **M** 5.4 surface-rupturing earthquake in Ernabella, South Australia (Clark *et al.*, 2014) indicated a very low stress drop (T. I. Allen, personal comm., 2015). Consequently, in developing new GMPEs for a region of Australia, Allen (2012) produced separate equations for shallow and deeper crustal earthquakes, the former yielding lower accelerations at all distances. The issue of stress drop and focal depth recently received considerable attention at the 2015 Seismological Society of America Annual Meeting. For example, Viegas *et al.* (2015) concluded that "on average, the reservoir events have low static and dynamic stress drops" (pp. 689) and Neighbors *et al.* (2015) report remarkably low stress drop (~3 bars) for induced earthquakes in Oklahoma, alluding to focal depth as a potential explanation. Boyd *et al.* (2015) also concluded "that stress drops are considerably lower for potentially induced earthquakes, possibly due to their relatively shallow focal depth" (pp. 690). Cramer (2015) concludes the primary reason for the low stress drops observed for induced earthquakes is focal depth and that for similar focal depths, induced and tectonic events may not be distinct. Wong *et al.* (2015) extend these arguments and note that "the shallow nature of induced earthquakes in a low-Q environment and the resulting potentially lower stress drops have also been recently suggested as a cause for lower

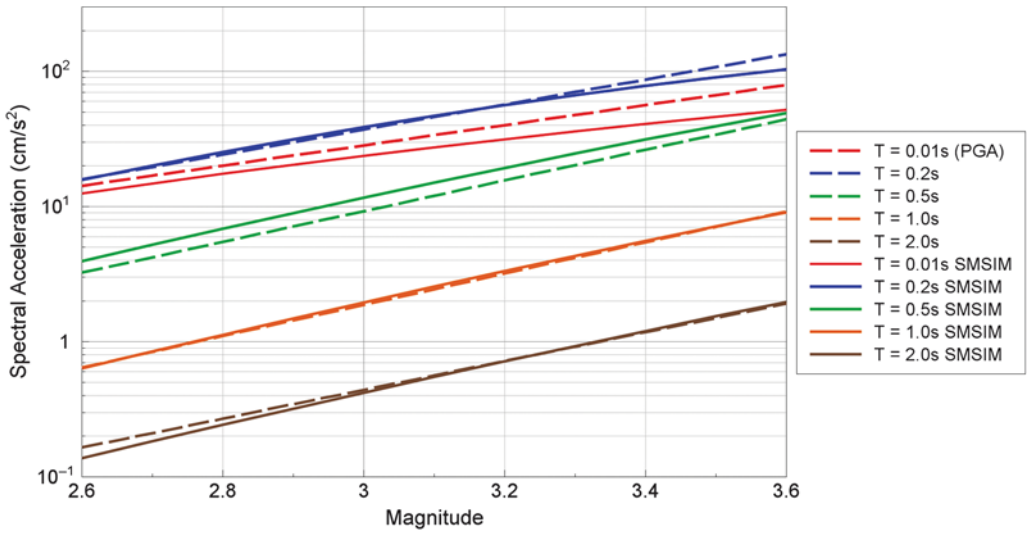

Figure 3. Comparison of simulated motions obtained with best-fit source, path, and site parameters with median predictions from empirical model of equation (1) as a function of magnitude, for an epicentral distance of 0 km.

ground motions as compared to tectonic earthquakes." Darragh *et al.* (2015) also find relatively low stress parameters for induced earthquakes in central and eastern North America. On the basis of such studies, the central model based on a stress parameter of 30 bars was judged to be a suitable best-estimate model and consequently assigned the highest weight (0.5, with 0.2 and 0.3 on the lower and upper models, respectively) in the logic-tree formulation.

Regressions for Parametric Equations

The final stage of the GMPE derivation for median predictions was to fit a functional form to the simulations. The functional form was chosen to be the same as equation (1) but with the addition of a nonlinear magnitude-scaling term that could take different values at small and large magnitudes:

$$\ln(Y) = c_1 + c_2\mathbf{M} + c_3(\mathbf{M} - \overline{M})^2 + c_4 \ln\sqrt{R_{\text{epi}}^2 + [\exp(c_5\mathbf{M} + c_6)]^2}, \qquad \mathbf{M} \le \overline{M}, \tag{2a}$$

$$\ln(Y) = c_1 + c_2\mathbf{M} + c_{3a}(\mathbf{M} - \overline{M})^2 + c_4 \ln\sqrt{R_{\text{epi}}^2 + [\exp(c_5\mathbf{M} + c_6)]^2}, \qquad \mathbf{M} > \overline{M}. \tag{2b}$$

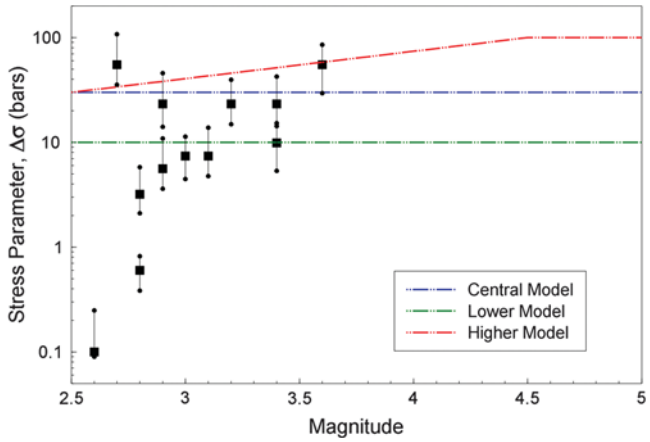

Figure 4. Individual stress parameter estimates, with vertical bars indicating confidence intervals using the procedure of Viegas *et al.* (2010), compared with the three stress parameter models defined for ground-motion simulations.

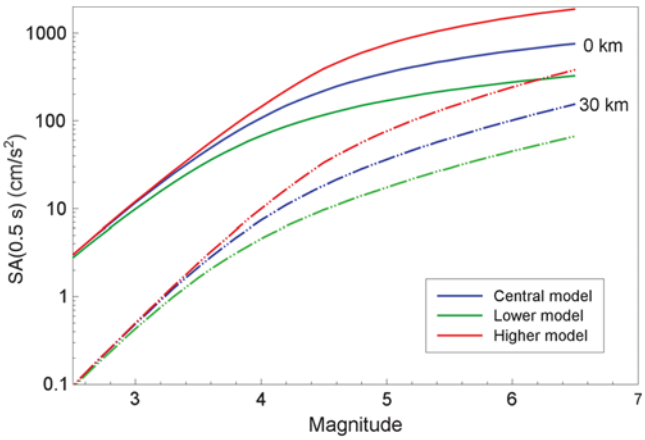

Figure 5. Predicted values of spectral acceleration (SA) at a response period of 0.5 s as a function of magnitude obtained with simulations using three different stress parameter models at epicentral distances of 0 and 30 km.

Table 1
Coefficients of Equation (2) for the Central ($\Delta\sigma = 30$ bars) Model

	SA(0.01 s)	SA(0.2 s)	SA(0.5 s)	SA(1.0 s)	SA(2.0 s)
c_1	1.1563	2.4972	−0.0684	−4.3882	−7.8093
c_2	1.2732	1.1216	1.5742	2.2288	2.6929
c_3	−0.3394	−0.4314	−0.5416	−0.3549	−0.1520
c_{3a}	−0.1342	−0.0747	−0.2397	−0.4202	−0.4370
c_4	−1.5048	−1.4806	−1.2266	−1.1640	−1.1526

SA, spectral acceleration.

Table 2
Coefficients of Equation (2) for the Lower ($\Delta\sigma = 10$ bars) Model

	SA(0.01 s)	SA(0.2 s)	SA(0.5 s)	SA(1.0 s)	SA(2.0 s)
c_1	1.0490	2.1812	0.6494	−3.2480	−7.1140
c_2	1.1122	1.0202	1.2775	1.8682	2.4569
c_3	−0.3132	−0.3408	−0.5417	−0.4377	−0.2117
c_{3a}	−0.0942	−0.0544	−0.1430	−0.3306	−0.4442
c_4	−1.4529	−1.4670	−1.2223	−1.1500	−1.1324

Table 3
Coefficients of Equation (2) for the Higher ($\Delta\sigma = 100$ bars) Model

	SA(0.01 s)	SA(0.2 s)	SA(0.5 s)	SA(1.0 s)	SA(2.0 s)
c_1	0.1638	1.5092	−1.7676	−5.9331	−8.5757
c_2	1.6566	1.4980	2.0695	2.6584	2.9277
c_3	−0.3236	−0.4312	−0.4308	−0.2273	−0.0983
c_{3a}	−0.2643	−0.2125	−0.4043	−0.5076	−0.4068
c_4	−1.5391	−1.4926	−1.2282	−1.1729	−1.1680

Simulations were performed for **M** 1.0–6.5 at 0.1 intervals and for 45 epicentral distances from 0 to 60 km (the maximum distance considered in the hazard and risk calculations). However, the regressions were performed only using simulated motions from **M** 2.5 and greater for two reasons: (1) smaller earthquakes do not make any significant contributions to the hazard or risk; and (2) the high kappa values associated with the soft-soil sites in the Groningen field lead to additional nonlinearity in the magnitude scaling for small earthquakes (e.g., Douglas and Jousset, 2011; Baltay and Hanks, 2014), which would require an additional break in the scaling or the inclusion of a cubic magnitude-scaling term.

In all cases, the coefficients c_5 and c_6, controlling the magnitude-dependent near-source distance saturation, were constrained to the values obtained from the initial empirical regressions (i.e., 0.4233 and −0.6083, respectively). Initially, the value of $\overline{M}$ was included as one of the parameters to be optimized in the fitting, but it was found that the value oscillated from period to period in a manner that could lead to irregular spectral shapes. For example, for the central model ($\Delta\sigma = 30$ bars), the values obtained for SAs at 0.01, 0.2, 0.5, 1.0, and 2.0 s were 4.7, 4.1, 5.0, 3.4, and 4.6. Using instead a fixed value of 4.5 at all periods—the same value used by Rietbrock *et al.* (2013) for the United Kingdom and Edwards and Fäh (2013) for Swiss simulations—results in only a very slight increase in the standard deviations and hence this was chosen as the constant value to be constrained in all the regressions. With the value of the hinge magnitude fixed at **M** 4.5 for all cases, the regressions were performed on the three sets of simulated ground motions corresponding to the central model and lower and higher alternatives. The coefficients are presented in Tables 1–3. The median predictions obtained from the regressions provide a very good approximation to the simulated values; Figure 6 shows the comparisons for the central model, but the results are very similar for the two other models as well.

Model for Aleatory Variability

In the development of GMPEs, the model for medians is only half the story. Equally important is the logarithmic standard deviation (sigma) of residuals that defines the probabilistic distribution of SAs that the equations predict. One of the shortcomings of stochastic GMPEs, as used to develop the median models for Groningen, is that, whereas sigma can be estimated by sampling probability density functions of the input source, path, and site parameters (e.g., Toro *et al.*, 1997), the results are difficult to defend due to the complex covariance of the simulation parameters, even when explicitly included in the simulations (e.g., Rietbrock *et al.*, 2013). In addition, the distinction between aleatory and epistemic components is often not clear using this approach. To overcome these limitations, stochastic models may be used to produce the median motions (relying on empirical data to define the sigma) and its component parts (e.g., Edwards and Fäh, 2013). In this section, the derivation of a sigma model for the Groningen GMPEs is described.

Residuals of Local Data

The first step is to examine the residuals of the local ground-motion data with respect to the models. Figure 7 shows the between- and within-event residuals of PGA with respect to the empirical model of equation (1) and also the residuals obtained with the formula of Abrahamson and Youngs (1992) for the same data with respect to the final model in equation (2a), using the coefficients of the central model (Table 1).

Although there are no discernible trends in the event terms with respect to magnitude, there are patterns in the within-event residuals with respect to distance; these are most likely related to unusual velocity structure above the gas reservoir (see the Discussion and Conclusions section). As far as the distributions of residuals with respect to equation (2) are concerned, we acknowledge that the small number of earthquakes in the current database may be insufficient to capture the full range of between-event variability τ.

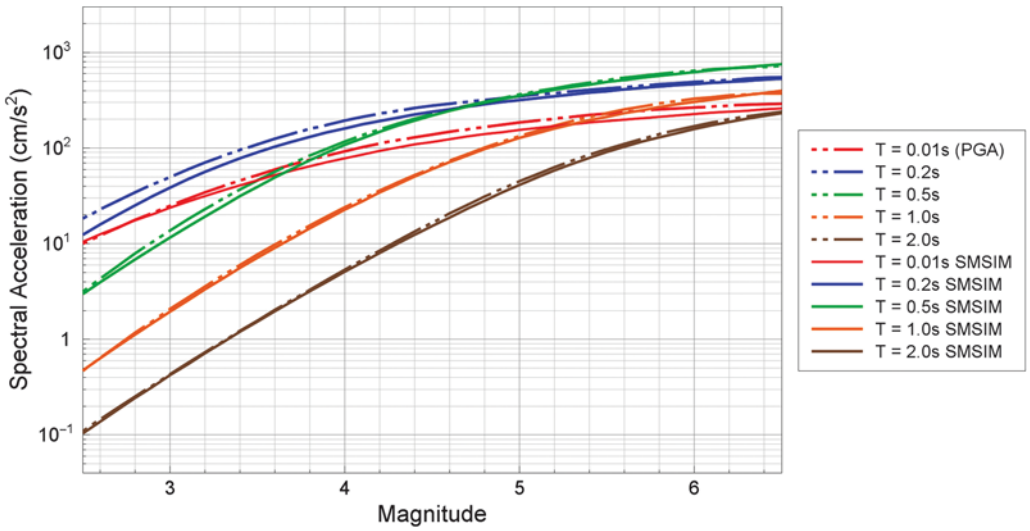

Figure 6. Comparison of median predictions from the final central ground-motion prediction equation (GMPE) with the ground motions obtained from the stochastic simulations at $R_{epi} = 0$ km as a function of magnitude.

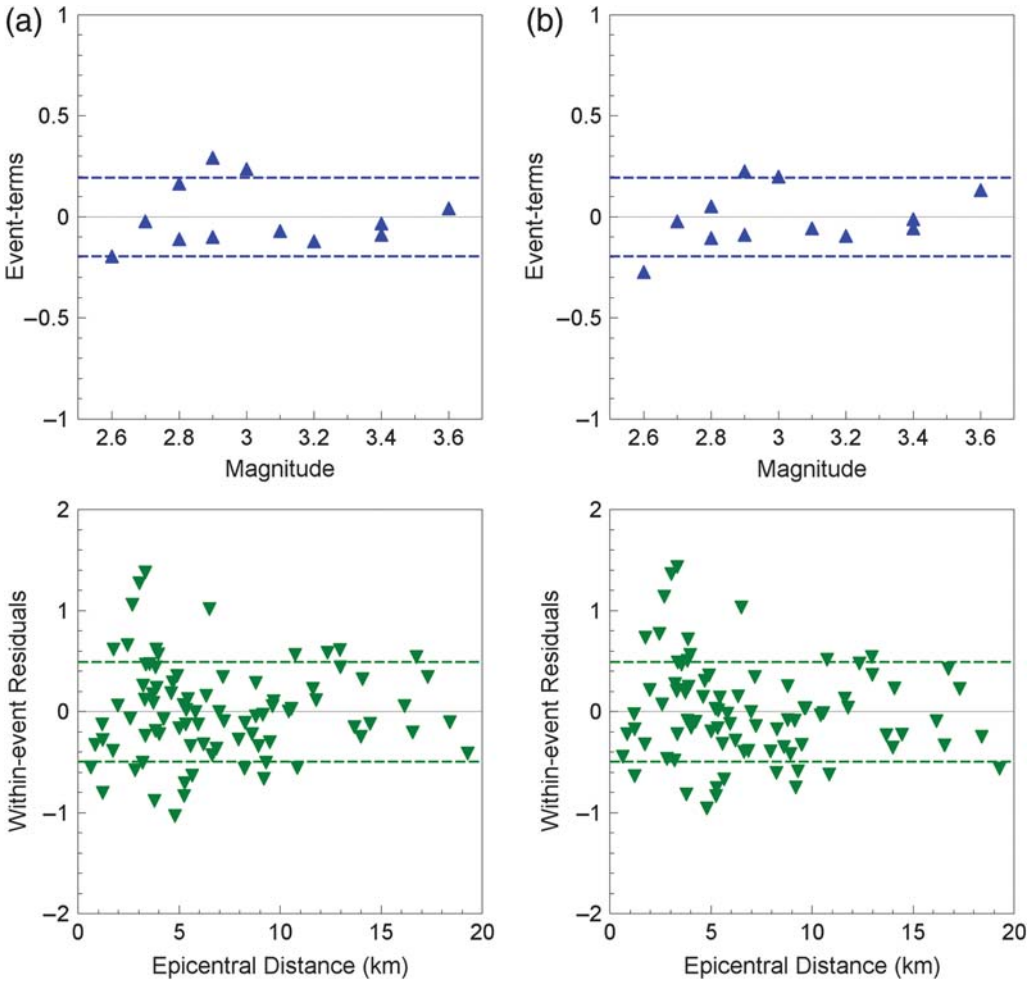

Figure 7. Between-event (upper) and within-event (lower) residuals, in natural logarithms, of the Groningen database with respect to (a) the empirical GMPE of equation (1) and (b) the final GMPE fit to the stochastic simulations using equation (2a). The dashed lines represent the standard deviations.

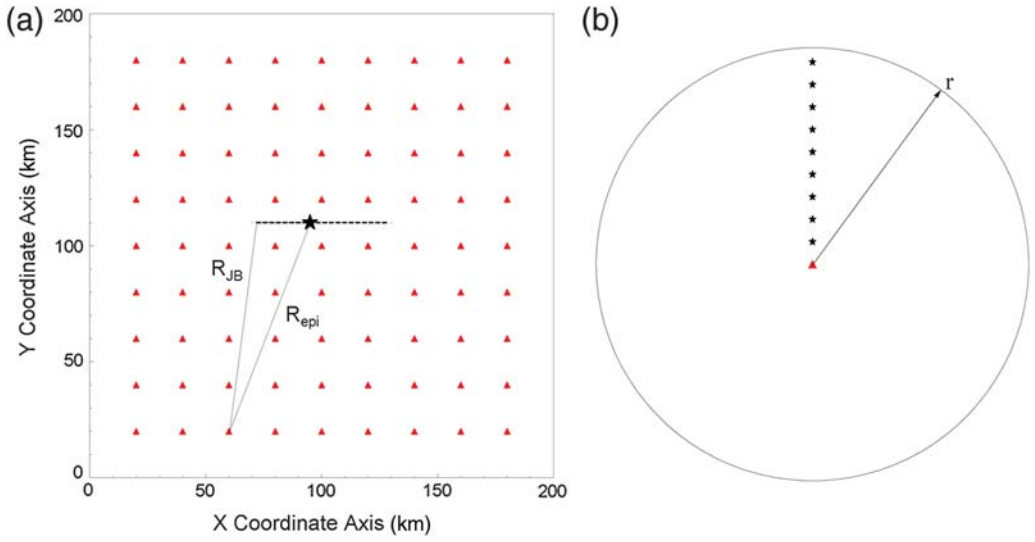

Figure 8. (a) Simulations envisaged by Akkar *et al.* (2014a,b) to estimate the additional variability in GMPEs based on R_{epi}. (b) Simplified formulation used in this study for a site (red triangle) at the center of a circular area, considering multiple epicentral locations within the circular source (black stars).

On the other hand, for a magnitude range of 1.1 units and distance range of 20 km, 85 records is not a sparse data sample, and the records also display a reasonably good distribution with respect to these two parameters (Fig. 2). In light of this, we are inclined to accept the measured within-event variability as a reliable estimate. However, because of the extrapolation to larger magnitudes, it was also necessary to consider whether adjustments need to be made. The first issue we considered is that the use of a point-source distance metric (R_{epi}), which was adopted as a tool of convenience in terms of computational efficiency in the preliminary hazard and risk models, will lead to underestimation of the variability for larger earthquakes and at sites close enough to the source to be influenced by the extent of the fault rupture. We therefore adopt the measured values from the Groningen data as the within-event variability for small magnitudes ϕ_{SM}, to which a correction $\delta\phi$, is required for the effect of the source extensions. The final sigma value is thus given by

$$\sigma = \sqrt{\tau^2 + (\phi_{SM}^2 + \delta\phi^2)}. \quad (3)$$

In the next section, we describe the derivation of the adjustment $\delta\phi$, after which the final sigma model is presented.

Adjustments for Point-Source Approximation

Akkar *et al.* (2014a,b) derived GMPEs in terms of both R_{epi} and Joyner–Boore distance R_{JB} and, surprisingly, found the sigma values for the two models to be quite similar. This was attributed to the sparseness of the database at short distances from larger earthquakes. Akkar *et al.* (2014a,b) proposed a computational exercise to derive the true sigma for the R_{epi} model using estimated motions from the R_{JB}-based model over a dense grid of observation points and then resampling these predictions in terms of R_{epi}, an objective that could also be met using the correlations between distance metrics proposed by Scherbaum *et al.* (2004). The approach adopted in this study is similar but computationally more efficient. The essence of the method is to simulate a large number of combinations of epicenter and receiver locations, as well as sampling a wide range of fault rupture lengths and orientations for earthquakes of different magnitudes. This is achieved by considering a single observation point and simulating different possible epicentral locations within a circular source zone (Fig. 8). We assumed vertical strike-slip fault rupture and the empirical relationship of Wells and Coppersmith (1994) to estimate the rupture length. We acknowledge that this empirical relationship derived from tectonic earthquake data may not be applicable to induced earthquakes at shallow depths (in part as a result of the lower effective crustal rigidity changing the relationship between seismic moment, rupture area, and fault displacement), but there are currently no equivalent relationships available for such events. The same procedure proposed here could equally be applied with another empirical relationship between magnitude and rupture dimensions (e.g., Clark *et al.*, 2014; Leonard, 2014; Stafford, 2014). To account for the variability in that empirical relationship, we used an equivalent five-point distribution based upon equating moments and using Gauss–Hermite quadrature (Miller and Rice, 1983). Using symmetry, it was sufficient to vary the rupture orientations through 90° in the simulations.

Figure 9 illustrates the calculation of the range of values of R_{JB} for a given R_{epi}, as a function of the fault orientation ϑ, rupture length L, and separation of the epicenter from the end of the rupture αL. The GMPEs of Akkar *et al.* (2014a,b) are then used to calculate the median values of SA for a single R_{epi} value and the range of corresponding R_{JB} values, from which the additional variance is then calculated. The

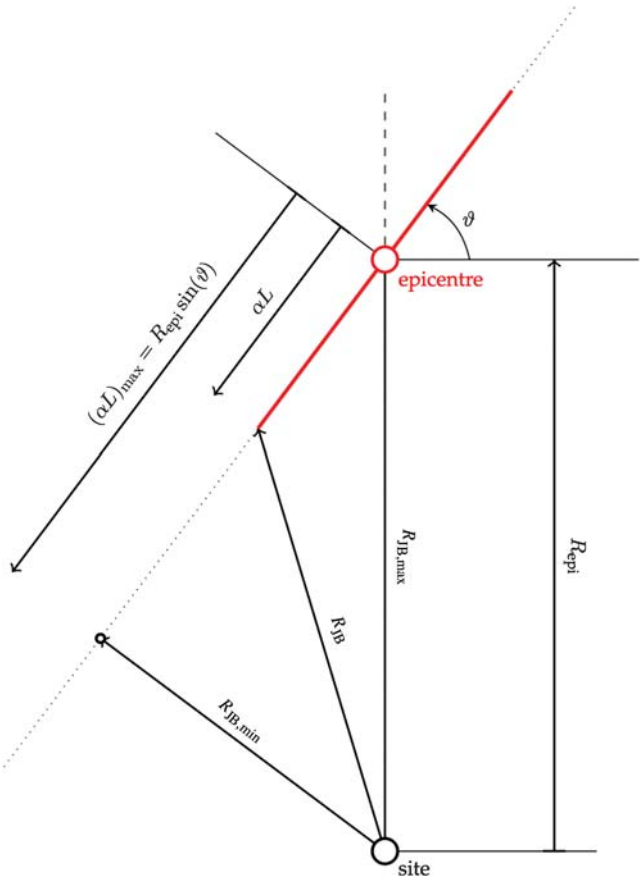

Figure 9. The geometry for calculating R_{epi} and Joyner–Boore distance (R_{JB}) for vertical strike-slip faults.

standard deviation required to adjust for the point-source approximation was then calculated in this way for a wide range of magnitudes and distances.

Figure 10 shows an example of the nature of the dependence on magnitude and distance, from which it can immediately be appreciated that as a function of the logarithm of distance, the functional form is remarkably similar to a Gaussian distribution. Taking advantage of this observation, the adjustment is modeled as follows:

$$\delta\phi = \mathrm{SF}\left(\frac{\varphi(z)}{\sigma_Z}\right), \qquad \mathbf{M} \geq 4 \quad \text{and} \quad R_{epi} > 0 \tag{4a}$$

$$\delta\phi = 0, \qquad \mathbf{M} < 4 \quad \text{or} \quad R_{epi} = 0, \tag{4b}$$

in which SF is the magnitude-dependent scaling factor, expressed as

$$\mathrm{SF} = \beta_1(\mathbf{M} - 4) + \beta_2(\mathbf{M} - 4)^2, \tag{5}$$

and $\varphi[\,]$ is the standard normal probability density function. The latter is given by the expression

$$\varphi(z) = \frac{1}{\sqrt{2\pi}}\exp\left(\frac{-z^2}{2}\right). \tag{6}$$

The argument of this expression is given by

$$z = \frac{\ln(R_{epi}) - \mu_Z}{\sigma_Z}, \tag{7}$$

and the parameters of this expression are given by

$$\mu_Z = \beta_3 + \beta_4(\mathbf{M} - 6.75) + \beta_5(\mathbf{M} - 6.75)^2 \tag{8}$$

and

$$\sigma_Z = \beta_6. \tag{9}$$

The coefficients are presented in Table 4 for the five chosen response periods.

Sigma Model

In order to capture the uncertainty in the sigma model, we once again propose a logic-tree formulation with three branches. Because the between-event component may be underestimated by the current database, the calculated values are taken as lower bounds. For the upper bound, we take the event terms from Akkar *et al.* (2014a,b), which was the basis for the preliminary GMPE developed for the field—because it is very unlikely that the earthquake-to-earthquake variability in the field could ever exceed that obtained from a study combining earthquakes from across Europe and the Middle East. The central values were simply assumed to lie midway between these two limits.

The sigma values are then calculated using equation (3), with the same within-event variability on all three branches. The values of τ and ϕ_{SM} are listed in Table 4, together with these coefficients. In closing, we note that several modern GMPEs invoke heteroskedastic models for sigma, in which the standard deviation is smaller for large-magnitude earthquakes than for smaller earthquakes (e.g., Abrahamson *et al.*, 2008; Strasser *et al.*, 2009). Confidence in our sigma model for the small magnitude range covered by the Groningen data could lead us to propose a decrease rather than an increase in sigma for larger magnitudes by invoking the patterns seen in such heteroskedastic sigma models or at least to offset the increase being modeled as the within-event variability penalty for using a point-source distance metric. However, instead we choose not to make any such reduction of the sigma explicitly, noting instead that the variability at larger magnitudes may actually be slightly greater than implied by our geometric penalty as a result of variability in the rupture process along the fault. Any reduction of sigma at larger magnitudes is therefore assumed to cancel out any excessive simplification in our adjustment model.

Rather than populate the logic tree with three median models and three sigma models, leading to nine possible com-

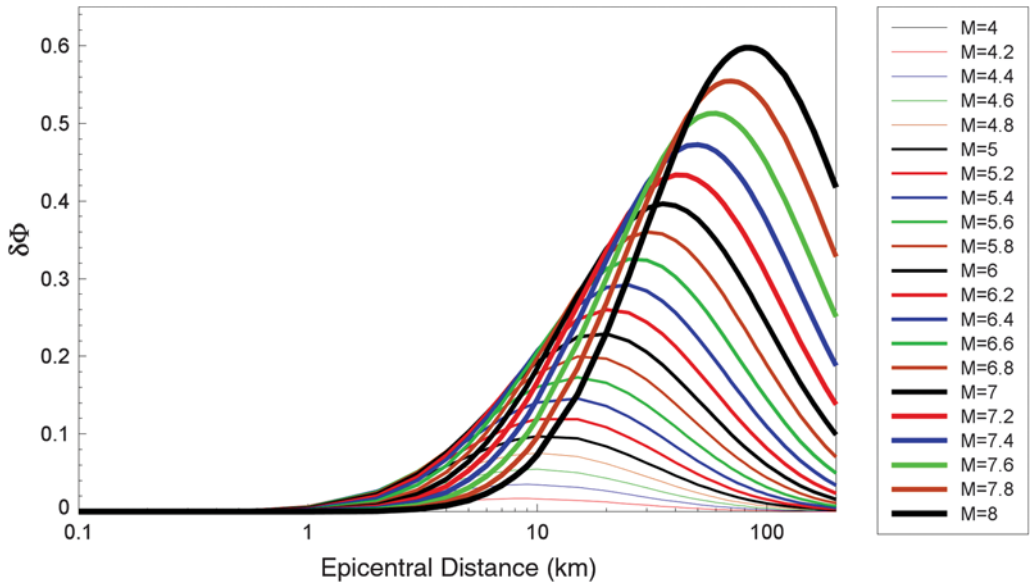

Figure 10. Calculated values of $\delta\phi$ for SA(0.5 s) as a function of magnitude and distance.

binations, and to ensure computational efficiency and a wide range of epistemic uncertainty, we proposed to join the high, central, and low estimates of both medians and sigmas into single branches (with the same weights indicated previously).

Figure 11 illustrates the behavior of the central model over a wide range of magnitudes, with curves for both median and 84th percentile values of SA at 0.2 s. The effect of the adjustment to the sigma value for the use of a point-source distance metric is seen to be modest for the largest magnitude of relevance to the Groningen hazard and risk assessment. The plot also shows the clear magnitude dependence of the attenuation as a result of the near-source distance saturation term.

Discussion and Conclusions

We presented the current state of development of GMPEs for application to the assessment of hazard and risk associated with induced seismicity in the Groningen gas field. Comparisons of the ground-motion predictions obtained from the models derived herein with those from other equations are almost *de rigueur* in papers presenting new GMPEs, even if the value of such comparisons may be rather limited, especially if multiple parameter adjustments are needed to create a common basis. Notwithstanding these reservations, we show some comparisons with the R_{hyp}-based model of Akkar *et al.* (2014a,b; hereafter referred as ASB14) because this GMPE, derived from tectonic earthquakes in Europe and the Middle East, has been used as the basis for preliminary seismic-hazard assessments in the Groningen field (e.g., Bourne *et al.*, 2015). Figures 12 and 13 show comparisons of median predictions from three equations derived in this study with those from the European GMPE, adopting a constant focal depth of 3 km, a V_{S30} value of 200 m/s, and normal faulting for the latter. The comparisons are shown for magnitudes that are relevant to the hazard and risk estimates in the Groningen field, namely **M** 4 and 5.5. In both cases, at shorter oscillator periods, ASB14 predicts motions that are

Table 4
Coefficients of Equations (3)–(9) for the Standard Deviations of the Predictions

	SA(0.01 s)	SA(0.2 s)	SA(0.5 s)	SA(1.0 s)	SA(2.0 s)
τ_{low}	0.2039	0.2514	0.2467	0.3612	0.3359
τ_{center}	0.2810	0.3337	0.3216	0.3789	0.3547
τ_{high}	0.3581	0.416	0.3965	0.3965	0.3734
ϕ_{SM}	0.4918	0.4454	0.5146	0.4081	0.4133
β_1	0.20380	0.20284	0.20761	0.21116	0.21290
β_2	0.073419	0.080624	0.044808	0.018152	0.005130
β_3	3.39511	3.39511	3.39511	3.39511	3.39511
β_4	0.70978	0.70978	0.70978	0.70978	0.70978
β_5	0.0900446	0.0900446	0.0900446	0.0900446	0.0900446
β_6	1.03275	1.03275	1.03275	1.03275	1.03275

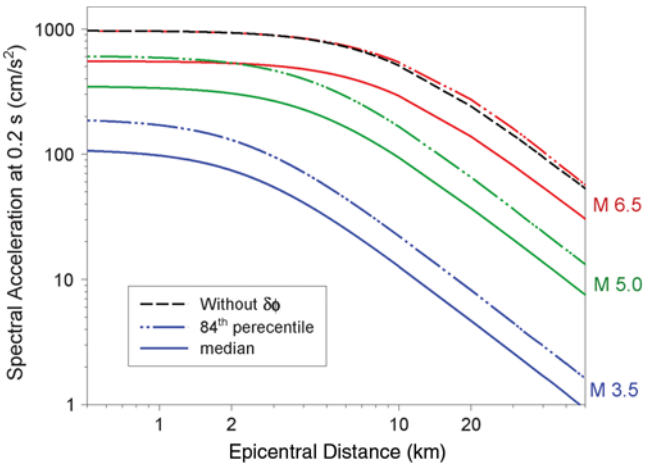

Figure 11. Median and 84th percentile predictions of SA (0.2 s) from the central model as a function of epicentral distance for three magnitudes; for the largest magnitude, the black dashed line indicates the effect of not including the point-source adjustment to the sigma value.

comparable with the upper model, which is consistent with the rationale behind the selection of the higher stress parameter of 100 bar. This observation is noteworthy because it is the case despite the large magnitude-dependent near-source distance saturation term in ASB14 (7.5 km) and the fact that ASB14 models nonlinear site response. The patterns seen at longer periods, where the ASB14 predictions seem relatively less severe than the Groningen-specific model, may in part reflect the influence of the deep soil deposits encountered in the field. The larger standard deviations associated with the ASB14 equations should also be taken into account in the interpretation of these comparisons.

There are several aspects of the new model for Groningen currently undergoing improvement and further developments, which will be presented subsequently, the most urgent of which is to incorporate site response effects into the model. The models presented herein have two weaknesses in this regard. The first is that they represent a network-average site amplification function and assume that this is a surrogate for the field-wide amplification function. The second, and potentially more serious, shortcoming is that this site amplification function is extrapolated linearly to larger magnitudes, which is almost certainly leading to conservative ground-motion estimates. NAM is leading a major program of work that is currently underway to construct a detailed velocity model for the entire field to characterize the nonlinear response of near-surface layers with respect to a reference horizon (likely to be the base of the Upper North Sea formation, located at an average depth of some 350 m) and to incorporate these into the predictive model. This will likely to be done through a zonation of the field into areas for which a representative site amplification function can be defined. This reinforces the advantages of developing models without any requirement for being

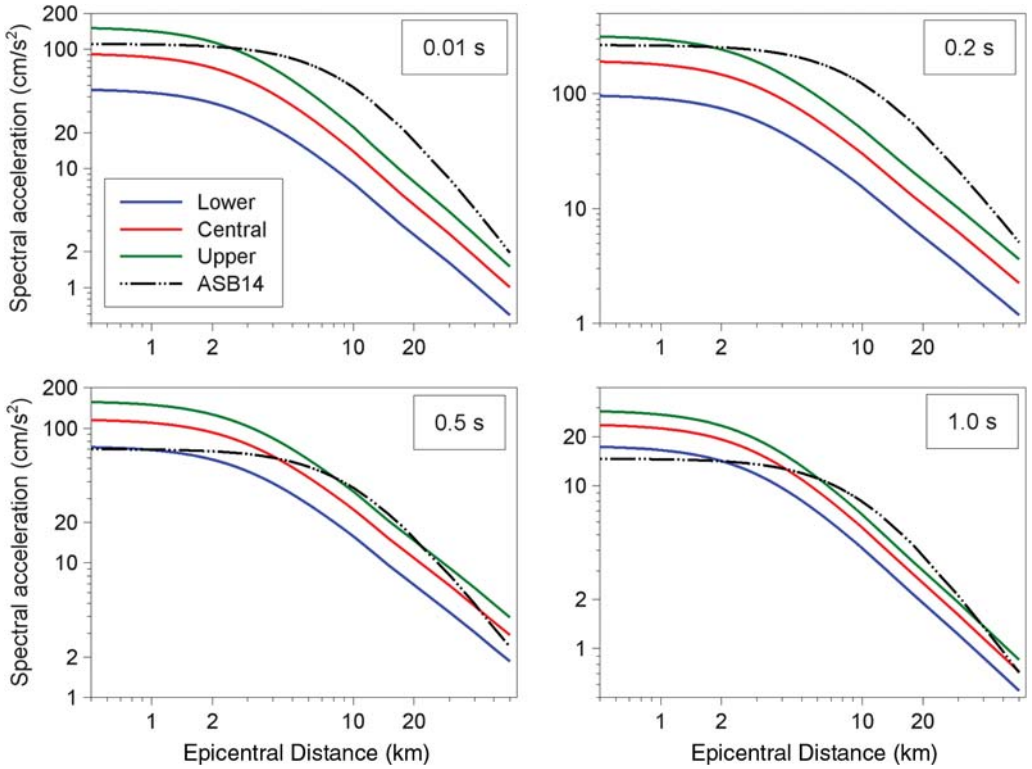

Figure 12. Comparison of median predictions of SAs at four response periods from the three Groningen-specific models and the ASB14 equation for European earthquakes, as a function of epicentral distance, for moment magnitude **M** 4.0. V_{S30} is set to 200 m/s in the ASB14 equation.

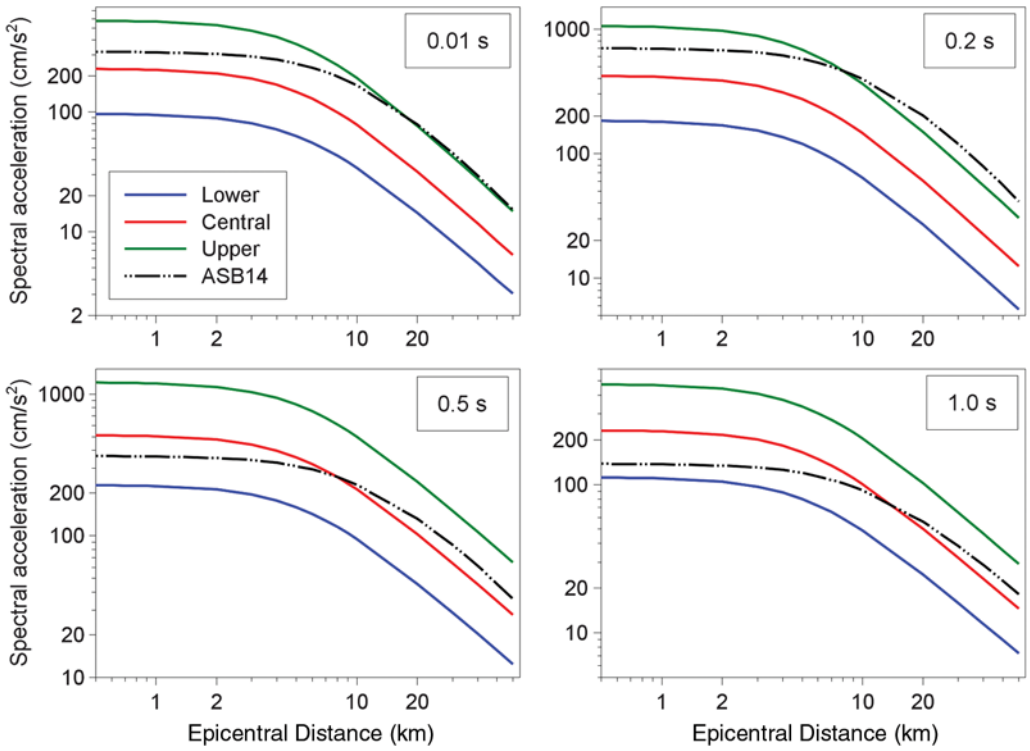

Figure 13. Comparison of median predictions of SAs at four response periods from the three Groningen-specific models and the ASB14 equation for European earthquakes, as a function of epicentral distance, for moment magnitude **M** 5.5. V_{S30} is set to 200 m/s in the ASB14 equation.

transportable to different applications, which can obviate the need to use simplified surrogate parameters such as V_{S30}.

Another important refinement relates to capturing the influence of the high-velocity Zechstein layer above the gas reservoir, which exerts a profound influence on the propagation of seismic waves (Kraaijpoel and Dost, 2013). The refraction and reflection of wavepaths departing from the seismic source with exit angles much different from zero leads to rapid attenuation over relatively short distances. The effect is seen in the relationship between amplitudes and durations of the recorded motions in the field, whereby those at short epicentral distances exhibit relatively high amplitudes associated with very short durations; in contrast, at greater distances the motions are of very low amplitude but the multiple ray paths lead to prolonged durations (Fig. 14). Full waveform simulations using finite differences and a detailed velocity model of the field will be used to constrain the geometric spreading model in the next refinement and are expected to lead to improvement in the residual patterns with epicentral distance seen with regard to the current model (Fig. 7).

Notwithstanding the need for these improvements, particularly the former, we believe that the approach used to develop these models may be useful to those faced with estimating ground motions from induced earthquakes in other locations. The capture of epistemic uncertainty through the use of simulations with distinct source parameters—as also proposed by Douglas *et al.* (2013)—is more transparent and tractable than populating a logic tree with multiple models, some of which may be of questionable applicability to the project in question (Atkinson *et al.*, 2014). However, the work presented herein also demonstrates the enormous value of local monitoring networks for induced seismicity, without which very large ranges of epistemic uncertainty need to be accommodated in the model.

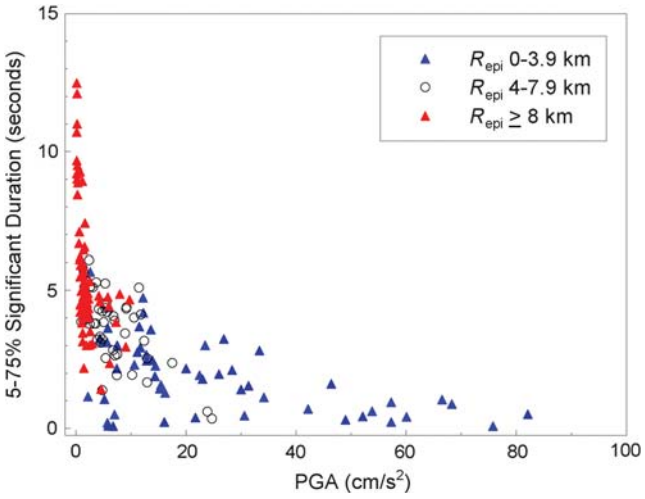

Figure 14. Peak ground acceleration (PGA) and significant durations of individual horizontal components of the Groningen ground motions, grouped in ranges of epicentral distances.

Finally, in the GMPEs presented herein, a distance metric has been used that is measured relative to a point-source representation of the earthquake source. Such an approach may often be used for induced-seismicity applications, because it is computationally efficient and may be considered acceptable in view of the relatively small magnitudes of the earthquakes considered. However, PSHAs and risk analyses are likely to also include integrations up to much larger magnitudes, given the difficulty in constraining the maximum possible earthquake that may be induced (which is compounded by the possibility of triggered seismicity). The application of GMPEs using distance metrics defined relative to extended fault ruptures in combination with a seismicity model representing individual earthquakes as hypocenters will result in systematic underestimation of hazard for larger magnitudes (e.g., Monelli *et al.*, 2014). Using GMPEs based on R_{epi} or R_{hyp} in association with such seismicity models is therefore internally consistent (Bommer and Akkar, 2012); however, at larger magnitudes the sigma values calculated from small-magnitude data need to be adjusted for the point-source approximation. In this article, we presented a formulation for this adjustment, which is generic and could be applied to other situations. For the case of Groningen, however, we are also developing new GMPEs based on R_{JB}, following the procedure suggested by Boore (2009), and will be conducting sensitivity analyses using seismicity models simulating hypocenters and fault ruptures. Each of these will be applied with the consistent GMPE to ascertain if the approximation of point sources is leading to bias in the risk estimates.

Data and Resources

The recordings used in this study were obtained from the Groningen accelerograph network operated by the Royal Dutch Meteorological Institute (KNMI). An expanded database, including more recent events and reprocessed accelerograms, together with an updated database of metadata for the recordings, will be made publicly available. Data from the KNMI network are now available from http://rdsa.knmi.nl (last accessed November 2015). The stochastic ground-motion simulations were performed using the software SMSIM (Boore, 2005).

Acknowledgments

The authors are indebted to many individuals for valuable discussion and feedback at different stages of the development of this work, including in particular Steve Oates and Stephen Bourne of Shell and Helen Crowley and Rui Pinho, with whom we defined the application requirements for the equations. Numerous other individuals also contributed valuable insights and ideas, particularly with regard to the ongoing development of this work, among whom we would like to particularly mention Pauline Kruiver from Deltares; Sara Minisini, Diego de Lazzari, Fons ten Krode, Alexander Droujinine, and Ewoud van Dedem from Shell; Remco Romijn from Nederlandse Aardolie Maatschappij B.V. (NAM); Adrian Rodriguez-Marek from Virginia Tech; and Dirk Kraaijpoel from Royal Dutch Meteorological Institute (KNMI). The original manuscript was significantly improved through constructive review comments by Associate Editor Ivan Wong and Reviewers Trevor Allen, Hilmar Bungum, Bob Darragh, John Douglas, and Jonathan Stewart, for which we are very grateful.

References

Abrahamson, N. A., and R. R. Youngs (1992). A stable algorithm for regression analyses using the random effects model, *Bull. Seismol. Soc. Am.* **82,** no. 1, 505–510.

Abrahamson, N. A., G. Atkinson, D. M. Boore, Y. Bozorgnia, K. Campbell, B. Chiou, I. M. Idriss, W. Silva, and R. Youngs (2008). Comparison of the NGA ground-motion relations, *Earthq. Spectra* **24,** no. 1, 45–66.

Akkar, S., M. A. Sandıkkaya, and J. J. Bommer (2014a). Empirical ground-motion models for point- and extended-source crustal earthquake scenarios in Europe and the Middle East, *Bull. Earthq. Eng.* **12,** no. 1, 359–387.

Akkar, S., M. A. Sandıkkaya, and J. J. Bommer (2014b). Erratum to "Empirical ground-motion models for point- and extended-source crustal earthquake scenarios in Europe and the Middle East," *Bull. Earthq. Eng.* **12,** no. 1, 389–390.

Allen, T. I. (2012). *Stochastic Ground Motion Prediction Equations for Southeastern Australian Earthquakes Using Updated Source and Attenuation Parameters*, Record 2012/69, Geoscience Australia, Canberra, Australia.

Allen, T. I., T. Dhu, P. R. Cummins, and J. F. Schneider (2006). Empirical attenuation of ground-motion spectral amplitudes in southwestern Western Australia, *Bull. Seismol. Soc. Am.* **96,** 572–585.

Anderson, J. G., and S. E. Hough (1984). A model for the shape of the Fourier amplitude spectrum of acceleration at high frequencies, *Bull. Seismol. Soc. Am.* **74,** 1969–1993.

Atkinson, G. M. (2006). Single-station sigma, *Bull. Seismol. Soc. Am.* **96,** 446–455.

Atkinson, G. M. (2015). Ground-motion prediction equation for small-to-moderate events at short hypocentral distances, with applications to induced-seismicity hazard, *Bull. Seismol. Soc. Am.* **105,** no. 2A, 981–992.

Atkinson, G. M., and M. Morrison (2009). Observations on regional variability in ground-motion amplitude for small-to-moderate magnitude earthquakes in North America, *Bull. Seismol. Soc. Am.* **99,** no. 4, 2393–2409.

Atkinson, G. M., J. J. Bommer, and N. A. Abrahamson (2014). Alternative approaches to modeling epistemic uncertainty in ground motion in probabilistic seismic-hazard analysis, *Seismol. Res. Lett.* **85,** no. 6, 1141–1144.

Bachmann, C. E., S. Wiemer, J. Woessner, and S. Hainzl (2011). Statistical analysis of the induced Basel 2006 earthquake sequence: Introducing a probability-based monitoring approach for enhanced geothermal systems, *Geophy. J. Int.* **186,** 793–807.

Baltay, A. S., and T. C. Hanks (2014). Understanding the magnitude dependence of PGA and PGV in NGA-West 2 data, *Bull. Seismol. Soc. Am.* **104,** no. 6, 2851–2865.

Bommer, J. J., and S. Akkar (2012). Consistent source-to-site distance metrics in ground-motion prediction equations and seismic source models for PSHA, *Earthq. Spectra* **28,** no. 1, 1–15.

Bommer, J. J., H. Crowley, and R. Pinho (2015). A risk-mitigation approach to the management of induced seismicity, *J. Seismol.* **19,** no. 2, 623–464.

Bommer, J. J., S. Oates, J. M. Cepeda, C. Lindholm, J. F. Bird, R. Torres, G. Marroquín, and J. Rivas (2006). Control of hazard due to seismicity induced by a hot fractured rock geothermal project, *Eng. Geol.* **83,** no. 4, 287–306.

Bommer, J. J., P. J. Stafford, J. E. Alarcón, and S. Akkar (2007). The influence of magnitude range on empirical ground-motion prediction, *Bull. Seismol. Soc. Am.* **97,** no. 6, 2152–2170.

Boore, D. M. (1983). Stochastic simulation of high-frequency ground motion based on seismological models of the radiated spectra, *Bull. Seismol. Soc. Am.* **73,** 1865–1894.

Boore, D. M. (2003). Simulation of ground motion using the stochastic method, *Pure Appl. Geophys.* **160,** 635–676.

Boore, D. M. (2005). SMSIM–Fortran programs for simulating ground motions from earthquakes: Version 2.3—A revision of OFR 96-80, *U.S. Geol. Surv. Open-File Rept. 00-509*, 55 pp.

Boore, D. M. (2009). Comparing stochastic point-source and finite-source ground-motion simulations: SMSIM and EXSIM, *Bull. Seismol. Soc. Am.* **99,** 3202–3216.

Bourne, S. J., S. J. Oates, J. J. Bommer, B. Dost, J. van Elk, and D. Doornhof (2015). A Monte Carlo method for probabilistic hazard assessment of induced seismicity due to conventional natural gas production, *Bull. Seismol. Soc. Am.* **105,** no. 3, 1721–1738.

Bourne, S. J., S. J. Oates, J. van Elk, and D. Doornhof (2014). A seismological model for earthquakes induced by fluid extraction from a subsurface reservoir, *J. Geophys. Res.* **119,** no. 12, 8991–9015, doi: 10.1002/2014JB011663.

Boyd, O. S., D. McNamara, S. Hartzell, and G. Choy (2015). A comparison of stress drop between tectonic and potentially induced earthquakes in the CEUS (abstract), *Seismol. Res. Lett.* **86,** no. 2B, 690.

Brune, J. N. (1970). Tectonic stress and the spectra of seismic shear waves from earthquakes, *J. Geophys. Res.* **75,** no. 26, 4997–5009.

Brune, J. N. (1971). Correction to "Tectonic stress and the spectra of seismic shear waves from earthquakes," *J. Geophys. Res.* **76,** no. 20, 5002.

Chiou, B., R. Youngs, N. Abrahamson, and K. Addo (2010). Ground-motion attenuation model for small-to-moderate shallow crustal earthquakes in California and its implications on regionalization of ground-motion prediction models, *Earthq. Spectra* **26,** no. 4, 907–926.

Clark, D., A. McPherson, T. Allen, and M. De Kool (2014). Coseismic surface deformation caused by the 23 March 2012 M_w 5.4 Ernabella (Pukatja) earthquake, central Australia: Implications for fault scaling relations in cratonic settings, *Bull. Seismol. Soc. Am.* **104,** 24–39.

Convertito, V., N. Maercklin, N. Sharma, and A. Zollo (2012). From induced seismicity to direct time-dependent seismic hazard, *Bull. Seismol. Soc. Am.* **102,** no. 6, 2563–2573.

Cotton, F., G. Pousse, F. Bonilla, and F. Scherbaum (2008). On the discrepancy of recent European ground-motion observations and predictions from empirical models: Analysis of KiK-net accelerometric data and point-sources stochastic simulations, *Bull. Seismol. Soc. Am.* **98,** no. 5, 2244–2261.

Cramer, C. H. (2015). Are ENA potentially induced earthquakes different from natural earthquakes? (abstract), *Seismol. Res. Lett.* **86,** no. 2B, 690.

Darragh, B., N. A. Abrahamson, W. J. Silva, and N. Gregor (2015). Development of hard rock ground-motion models for Region 2 of central and eastern North America, in *NGA-East: Median Ground-Motion Models for the Central and Easterm North America Region*, PEER Report 2015/04, Pacific Earthquake Engineering Research Center, University of California, Berkeley, California, 51–84.

Deichmann, N. (2006). Local magnitude, a moment revisited, *Bull. Seismol. Soc. Am.* **96,** 1267–1277.

Dost, B., T. van Eck, and H. Haak (2004). Scaling of peak ground acceleration and peak ground velocity recorded in The Netherlands, *Bollettino di Geofisica Teorica ed Applicata* **45,** no. 3, 153–168.

Douglas, J., and H. Aochi (2014). Using estimated risk to develop stimulation strategies for enhanced geothermal systems, *Pure Appl. Geophys.* **171,** 1847–1858.

Douglas, J., and P. Jousset (2011). Modeling the difference in ground-motion magnitude-scaling in small and large earthquakes, *Seismol. Res. Lett.* **82,** no. 4, 504–508.

Douglas, J., B. Edwards, V. Convertito, N. Sharma, A. Tramelli, D. Kraaijpoel, B. Mena Cabrera, N. Maercklin, and C. Troise (2013). Predicting ground motion from induced earthquakes in geothermal areas, *Bull. Seismol. Soc. Am.* **103,** no. 3, 1875–1897.

Edwards, B., and D. Fäh (2013). A stochastic ground-motion model for Switzerland, *Bull. Seismol. Soc. Am.* **103,** 78–98.

Edwards, B., A. Rietbrock, J. J. Bommer, and B. Baptie (2008). The acquisition of source, path, and site effects from micro-earthquake recordings using *Q* tomography: Application to the United Kingdom. *Bull. Seismol. Soc. Am.* **98,** 1915–1935.

Goertz-Allmann, B. P., B. Edwards, F. Bethmann, N. Deichmann, J. Clinton, D. Faeh, and D. Giardini (2011). A new empirical magnitude scaling relation for Switzerland, *Bull. Seismol. Soc. Am.* **101,** 3088–3095.

Grünthal, G., R. Wahlström, and D. Stromeyer (2009). The unified catalogue of earthquakes in central, northern, and northwestern Europe (CENEC) —Updated and expanded to the last millennium, *J. Seismol.* **13,** no. 4, 517–154, doi: 10.1007/s10950-008-9144-9.

Hanks, T. C., and R. K. McGuire (1981). The character of high-frequency ground motion, *Bull. Seismol. Soc. Am.* **71,** no. 6, 2071–2095.

Häring, M. O., U. Schanz, F. Ladner, and B. C. Dyer (2008). Characterisation of the Basel 1 enhanced geothermal system, *Geothermics* **37,** 469–495.

Herrmann, R. B. (1985). An extension of random vibration theory estimates of strong ground motion to large distances, *Bull. Seismol. Soc. Am.* **75,** 1447–1453.

Hough, S. E. (2014). Shaking from injection-induced earthquakes in the central and eastern United States, *Bull. Seismol. Soc. Am.* **104,** no. 5, 2619–2626.

Kraaijpoel, D., and B. Dost (2013). Implications of salt-related propagation and mode conversion effects on the analysis of induced seismicity, *J. Seismol.* **17,** no. 1, 95–107.

Leonard, M. (2014). Self-consistent earthquake fault-scaling relations: Update and extension to stable continental strike-slip faults, *Bull. Seismol. Soc. Am.* **104,** no. 6, 2953–2965.

Lin, P.-S., B. S.-J. Chiou, N. A. Abrahamson, M. Walling, C.-T. Lee, and C.-T. Cheng (2011). Repeatable source, site, and path effects on the standard deviation for empirical ground-motion prediction models, *Bull. Seismol. Soc. Am.* **101,** 2281–2295.

Majer, E., J. Nelson, A. Robertson-Tait, J. Savy, and I. Wong (2012). *Protocol for Addressing Induced Seismicity Associated with Enhanced Geothermal Systems, DOE/EE-0662*, U.S. Department of Energy.

Mena, B., S. Wiemer, and C. Bachmann (2013). Building robust models to forecast induced seismicity related to geothermal reservoir enhancement, *Bull. Seismol. Soc. Am.* **103,** no. 1, 383–393.

Mignan, A., D. Landtwing, B. Mena, and S. Wiemer (2015). Induced seismicity risk assessment for the 2006 Basel, Switzerland, enhanced geothermal system project: Role of parameter uncertainty on risk mitigation, *Geothermics* **53,** 133–146.

Miller, A. C., and T. R. Rice (1983). Discrete approximations of probability distributions, *Manag. Sci.* **29,** 352–362.

Monelli, D., M. Pagani, G. Weatherill, L. Danciu, and J. Garcia (2014). Modeling distributed seismicity for probabilistic seismic-hazard analysis: Implementation and insights with the OpenQuake engine, *Bull. Seismol. Soc. Am.* **104,** 1636–1649.

Neighbors, C., E. S. Cochran, G. M. Atkinson, and K. M. Keranen (2015). Low stress drops observed for the 2011 M 5.7 Prague, Oklahoma, earthquake sequence (abstract), *Seismol. Res. Lett.* **86,** no. 2B, 725.

Pinheiro, J. C., and D. M. Bates (2004). *Mixed-Effects Models in S and S-PLUS*, Springer-Verlag, New York, 548 pp.

Rietbrock, A., F. Strasser, and B. Edwards (2013). A stochastic earthquake ground-motion prediction model for the United Kingdom, *Bull. Seismol. Soc. Am.* **103,** 57–77.

Rodriguez-Marek, A., F. Cotton, N. Abrahamson, S. Akkar, L. Al-Atik, B. Edwards, G. Montalva, and H. Mousad (2013). A model for single-station standard deviation using data from various tectonic regions, *Bull. Seismol. Soc. Am.* **103,** 3149–3163.

Scherbaum, F., J. Schmedes, and F. Cotton (2004). On the conversion of source-to-site distance measures for extended earthquake source models, *Bull. Seismol. Soc. Am.* **94,** 1053–1069.

Sharma, N., V. Convertito, N. Maercklin, and A. Zollo (2013). Ground-motion prediction equations for The Geysers geothermal area based on induced seismicity records, *Bull. Seismol. Soc. Am.* **103,** no. 1, 117–130.

Stafford, P. J. (2014). Source-scaling relationships for the simulation of rupture geometry within probabilistic seismic-hazard analysis, *Bull. Seismol. Soc. Am.* **104,** no. 4, 1620–1634.

Strasser, F. O., N. A. Abrahamson, and J. J. Bommer (2009). Sigma: Issues, insights, and challenges, *Seismol. Res. Lett.* **80,** no. 1, 40–56.

Toro, G. R., N. A. Abrahamson, and J. F. Schneider (1997). Model of strong ground motions from earthquakes in central and eastern North America: Best estimates and uncertainties, *Seismol. Res. Lett.* **68,** no. 1, 41–57.

Viegas, G., R. E. Abercrombie, and W.-Y. Kim (2010). The 2002 M 5 Au Sable Forks, NY, earthquake sequence: Source scaling relationships and energy budget, *J. Geophys. Res.* **115,** no. B07310, doi: 10.1029/2009JB006799.

Viegas, G., T. Urbanic, and A. Baig (2015). Are source characteristics of fluid driven hydraulic fracture induced earthquakes distinct from natural tectonic earthquakes? (abstract), *Seismol. Res. Lett.* **86,** no. 2B, 689.

Wells, D. L., and K. J. Coppersmith (1994). New empirical relationships among magnitude, rupture length, rupture width, rupture area, and surface displacement, *Bull. Seismol. Soc. Am.* **84,** 974–1002.

Wong, I., J. Bott, M. Dober, and P. Thomas (2015). Examination of the strong motion and broadband data for injection-induced earthquakes in the US (abstract), *Seismol. Res. Lett.* **86,** no. 2B, 692.

Yenier, E., and G. M. Atkinson (2014). Equivalent point-source modeling of moderate-to-large magnitude earthquakes and associated ground-motion saturation effects, *Bull. Seismol. Soc. Am.* **104,** no. 3, 1458–1478.

Zoback, M. D. (2012). Managing the seismic risk posed by waste water disposal, *EARTH Magazine* 57, no. 4, American Geosciences Institute, http://www.earthmagazine.org/article/managing-seismic-risk-posed-wastewater-disposal (last accessed July 2015).

Civil and Environmental Engineering
Imperial College London
South Kensington
London SW7 2AZ, United Kingdom
j.bommer@imperial.ac.uk
p.stafford@imperial.ac.uk
(J.J.B., P.J.S.)

Royal Netherlands Meteorological Institute (KNMI)
Utrechtseweg 297
3731GA De Bilt, The Netherlands
bernard.dost@knmi.nl
(B.D.)

Department of Earth, Ocean and Ecological Sciences
University of Liverpool
4 Brownlow Street
Liverpool L69 3GP, United Kingdom
ben.edwards@liverpool.ac.uk
(B.E.)

Nederlandse Aardolie Maatschappij B.V. (NAM)
Schepersmaat 2
9405 TA Assen, The Netherlands
Jan.Van-Elk@shell.com
dirk.doornhof@shell.com
(J.v., D.D.)

Independent Engineering Consultant
9D Kempsford Gardens
London SW5 9LA United Kingdom
michail.ntinalexis10@alumni.imperial.ac.uk
(M.N.)

Manuscript received 20 October 2015;
Published Online 29 December 2015